

Directly profiling the dark-state transition density via scanning tunneling microscope

Guohui Dong,¹ Zhubin Hu,² Xiang Sun,^{2,3,*} and Hui Dong^{1,†}

¹Graduate School of Chinese Academy of Engineering Physics, Beijing 100084, China

²New York University Shanghai and NYU-ECNU Center for

Computational Chemistry, 1555 Century Avenue, Shanghai 200122, China

³Department of Chemistry, New York University, New York, New York 10003, United States

The molecular dark state participates in many important photon-induced processes, yet is typically beyond the optical-spectroscopic measurement due to the forbidden transition dictated by the selection rule. In this work, we propose to use the scanning tunneling microscope (STM) as an incisive tool to directly profile the dark-state transition density of a single molecule, taking advantage of the localized static electronic field near the metal tip. The detection of dark state is achieved by measuring the fluorescence from a higher bright state to the ground state with assistant optical pumping. The current proposal shall bring new methodology to study the single-molecule properties in the electro-optical devices and the light-assisted biological processes.

Introduction – Controllable light-matter interaction in the nanometer scale is one of the most fundamental and attractive topics in areas such as laser techniques [1, 2], atom manipulation [3–6], and cavity quantum electrodynamics [7–9]. Typically, the wavelength of the optical field is several orders of magnitude larger than the size of the matter of interest. In this region, the systems are essentially manipulated under the dipole interaction $\vec{\mu} \cdot \vec{E}$, where $\vec{\mu}$ is the electric dipole of the matter and \vec{E} is the external electric field. Consequently, only the transitions between the atomic or molecular states with nonzero transition dipoles can be probed with electromagnetic field, leaving the dark state with zero transition dipole beyond the optical detection. For this reason, traditional optical spectroscopic approaches such as infrared [10], Raman [11], and fluorescence [12, 13] spectroscopies are not applicable for the detection of dark states. However, the molecular dark state plays a significant role in many biochemical processes, such as it helps to resist the photochemical damage to the deoxyribonucleic acid (DNA) induced by ultraviolet light [14] and assist in the energy transfer process in the photosynthetic systems [15, 16].

The straightforward method is to break the dipole approximation with the spatial modulated field on the scale comparable to a single molecule. Such modulated field can be found near the tip of the scanning tunneling microscope (STM), which is as small as several atoms and able to induce electronic excitation which would have been forbidden under the dipole approximation. In contrast to optical excitation, the electronic excitation induced in STM provides detailed information on molecular states [17, 18]. By counting the luminescence photon, the scanning-tunneling-microscope-induced luminescence (STML) has emerged as a crucial tool for studying photoelectronic properties of single molecules [19–25].

In this Letter, we show the scheme of directly profiling the dark-state transition details from STM [26] taking advantage of the localized electric field. We quantitatively demonstrate the resemblance between the relative

inelastic current (luminescence photon counting) and the transition density profile of the dark-state transition.

Model – We demonstrate the basic setup of the model in Fig. 1(a), where a single molecule is placed on a NaCl-covered metal substrate. A metal tip scans over the molecule to allow the profiling. Driven at a nonzero bias voltage, an electron tunnels from one electrode to the other, while interacting with the molecule through the Coulomb interaction.

The total Hamiltonian consists of the tunneling electron Hamiltonian \hat{H}_{el} , the molecular Hamiltonian \hat{H}_{m} , and the electron-molecule interaction Hamiltonian $\hat{H}_{\text{el-m}}$. The tunneling electron Hamiltonian is $\hat{H}_{\text{el}} = -\hat{\nabla}^2/(2m_e) + V(\hat{\mathbf{r}})$, where $V(\hat{\mathbf{r}})$ stands for the tunneling-electron potential at $\hat{\mathbf{r}} = (x, y, z)$ and m_e is the electron mass. The free tip and substrate wavefunctions are written as [26–30]

$$\hat{H}_{\text{el,t}} |\phi_k\rangle \simeq \tilde{\xi}_k |\phi_k\rangle, \quad (1a)$$

$$\hat{H}_{\text{el,s}} |\varphi_n\rangle \simeq \tilde{E}_n |\varphi_n\rangle, \quad (1b)$$

respectively. Here, $\hat{H}_{\text{el,t}}$ ($\hat{H}_{\text{el,s}}$) is the free tip (substrate) Hamiltonian without the corresponding potential in the substrate (tip) region. $|\phi_k\rangle$ ($|\varphi_n\rangle$) is the eigenfunction with eigenenergy $\tilde{\xi}_k \equiv \xi_k + eV_b$ ($\tilde{E}_n \equiv E_n$), and ξ_k (E_n) is its corresponding eigenenergy at zero bias voltage [26]. The molecular Hamiltonian is simplified as a multi-level system $\hat{H}_{\text{m}} = E_g |\chi_g\rangle \langle \chi_g| + \sum_{i=1}^l E_{e,i} |\chi_{e,i}\rangle \langle \chi_{e,i}|$, where $|\chi_g\rangle$ ($|\chi_{e,i}\rangle$) is its ground (i -th excited) state with energy E_g ($E_{e,i}$) and l is the total number of excited states.

The excitation of the molecules are performed through the electron-molecule interaction $\hat{H}_{\text{el-m}}$ [26] as

$$\begin{aligned} \hat{H}_{\text{el-m}} &\simeq - \sum_{i=1}^l \sum_{n,k} \mathcal{N}_{s,t;i|V_b,E_n \rightarrow \xi_k} |\phi_k\rangle \langle \varphi_n| \otimes \hat{\sigma}_{x,i} \\ &\simeq - \sum_{i=1}^l \sum_{n,k} \mathcal{N}_{t,s;i|V_b,\xi_k \rightarrow E_n} |\varphi_n\rangle \langle \phi_k| \otimes \hat{\sigma}_{x,i}, \quad (2) \end{aligned}$$

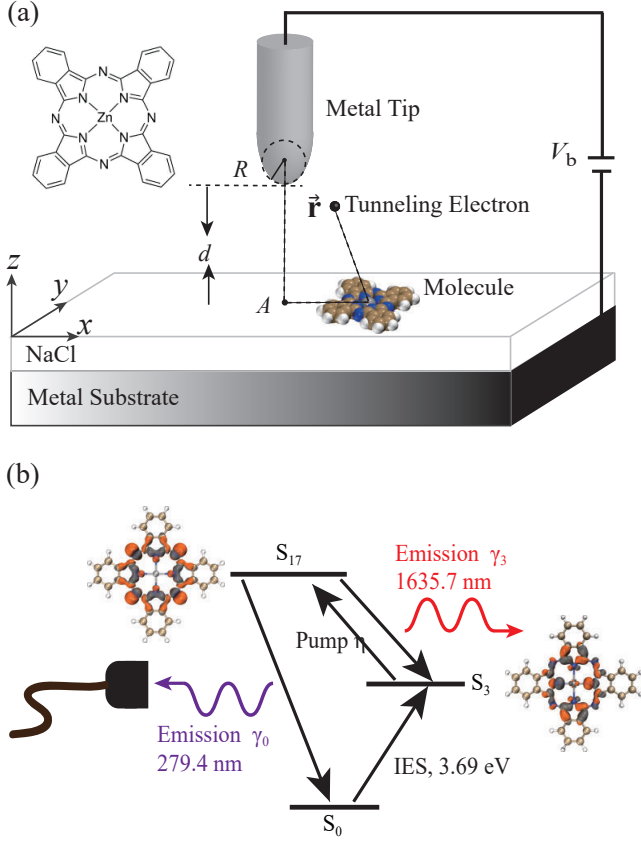


Figure 1. (Color online) (a) Schematic diagram of scanning-tunneling-microscope-induced luminescence (STML). A single molecule is placed on a NaCl-covered metal plane. The STM tip apex is treated as a sphere with radius R . Point A represents the projection position of tip's center on the plane, and d stands for the distance between the tip and plane. The tunneling electron is shown as a black sphere with vector \vec{r} , and the center position of the molecule is set as the origin of the reference frame. Inset: ZnPc molecule. (b) Schematic diagram of the detection of dark state S_3 . Both the transition dipole moments between S_0 - S_{17} and S_3 - S_{17} are nonzero. Firstly the molecule is excited to the dark state through the IES process and a laser with the wavelength 1635.7nm couples the dark state S_3 and the bright state S_{17} . The molecule in S_{17} emits photon through decaying to S_0 and S_3 . Photons at the wavelength 279.4nm are collected to profile the dark state. Insets: the transition density of transitions S_0 - S_{17} and S_0 - S_3 . The orange and gray parts represent the positive and negative transition density, respectively.

where the transition matrix element

$$\begin{aligned} \mathcal{N}_{s,t;i|V_b,E_n \rightarrow \xi_k} &= \mathcal{N}_{t,s;i|V_b,\xi_k \rightarrow E_n} \\ &= e^2 \int d^3\vec{q} \rho_{T,i}(\vec{q}) \rho_{n,k}(-\vec{q}) \frac{4\pi}{q^2} \end{aligned} \quad (3)$$

describes the transition matrix element from $|\phi_k\rangle$ ($|\varphi_n\rangle$) to $|\varphi_n\rangle$ ($|\phi_k\rangle$) in the subspace $|\chi_g\rangle, |\chi_{e,i}\rangle$, and $\hat{\sigma}_{x,i} \equiv |\chi_{e,i}\rangle\langle\chi_g| + |\chi_g\rangle\langle\chi_{e,i}|$ stands for the molecular transi-

tion. Here $\rho_{T,i}(\vec{q})$ and $\rho_{n,k}(\vec{q})$ are the Fourier transforms of the transition density $\rho_{T,i}(\vec{r}) \equiv \langle\vec{r}|\chi_{e,i}\rangle\langle\chi_g|\vec{r}\rangle$ and the product of the wavefunctions of the tip and the substrate $\rho_{n,k}(\vec{r}) \equiv \langle\vec{r}|\phi_k\rangle\langle\varphi_n|\vec{r}\rangle$, respectively. The transition dipole moment $\vec{\mu}_i$ is obtained as the integral of the transition density $\rho_{T,i}(\vec{r})$ and vector \vec{r} , i.e., $\vec{\mu}_i = \int d^3\vec{r} \rho_{T,i}(\vec{r}) \vec{r}$. Detailed derivation is provided in Supplementary Material. Beyond the dipole approximation, the transition matrix element here is expressed as a convolution of the Fourier transform of the transition density and the electrode wavefunctions.

The properties of the molecules can be described by the tunneling current and the photon counting. The tunneling current is calculated to the first order ($\hat{H}_{el} - \hat{H}_{el,s}$ and \hat{H}_{el-m} as the perturbation). At the negative bias $V_b < 0$, the molecule is initially in its ground state and the electron is in the substrate eigenstate, i.e., $|\Psi(t=0)\rangle = |\chi_g\rangle|\varphi_n\rangle$. The wavefunction at time t evolves as

$$\begin{aligned} |\Psi(t)\rangle &= e^{-i(\tilde{E}_n + E_g)t} |\chi_g\rangle|\varphi_n\rangle \\ &+ \sum_k \left[c_{g;k}(t) |\chi_g\rangle + \sum_{i=1}^l c_{e,i;k}(t) |\chi_{e,i}\rangle \right] |\phi_k\rangle. \end{aligned} \quad (4)$$

Here $c_{g;k}(t)$ shows the probability amplitude of the elastic tunneling process and $c_{e,i;k}(t)$ the probability amplitude of the inelastic tunneling process. In the rotating-wave approximation, the inelastic tunneling amplitude becomes

$$c_{e,i;k}(t) = \frac{e^{-i(\tilde{E}_n + E_g)t} - e^{-i(\tilde{\xi}_k + E_{e,i})t}}{\tilde{E}_n - \tilde{\xi}_k - E_{eg,i}} \mathcal{N}_{s,t;i|V_b,E_n \rightarrow \xi_k},$$

where $E_{eg,i} \equiv E_{e,i} - E_g$ is the energy gap between the molecular states $|\chi_g\rangle$ and $|\chi_{e,i}\rangle$. By tracing out the degrees of freedom of the molecule, we obtain the inelastic current from $|\varphi_n\rangle$ to $|\phi_k\rangle$ as $\mathcal{J}_{n \rightarrow k} = \sum_{i=1}^l d |c_{e,i;k}(t)|^2 / dt$ and the total inelastic current as

$$I_{-,inela} \simeq \sum_{i=1}^l I_{-,inela,i}, \quad (5)$$

where

$$\begin{aligned} I_{-,inela,i} &= 2\pi e \int_{\mu_0 + eV_b + E_{eg,i}}^{\mu_0} dE_n \rho_s(E_n) \rho_t(\xi_k) \\ &\times |\mathcal{N}_{s,t;i|V_b,E_n \rightarrow \xi_k}|^2 |_{\xi_k = E_n - eV_b - E_{eg,i}}. \end{aligned} \quad (6)$$

Here μ_0 is the Fermi energy of the electrode and $\rho_t(E)$ ($\rho_s(E)$) is the density of state of the tip (substrate) at energy E . With the inelastic current at both negative and positive bias, we obtain the inelastic current as below (for the inelastic current at positive bias, see Supplementary Material)

$$I_{inela} = \begin{cases} I_{-,inela}, & V_b < -\min\left[\frac{E_{eg,i}}{e}\right], \\ 0, & -\min\left[\frac{E_{eg,i}}{e}\right] \leq V_b \leq \min\left[\frac{E_{eg,i}}{e}\right], \\ I_{+,inela}, & V_b > \min\left[\frac{E_{eg,i}}{e}\right]. \end{cases} \quad (7)$$

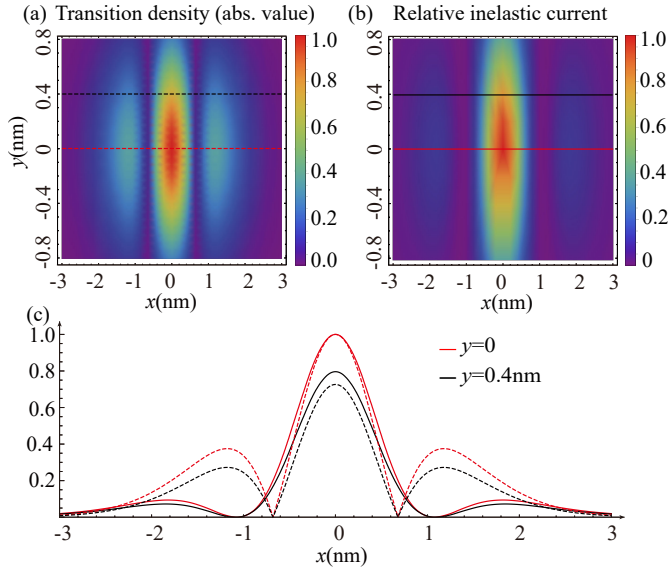


Figure 2. (Color online) (a,b) The 2D plot of relative transition density ($z = 0$) and inelastic current ($V_b = -2.5V$). (c) The relative transition density (dashed lines) and the relative inelastic current (solid lines) for $y = 0, 0.4nm$.

Here $\min [E_{eg,i}/e]$ means the minimal $E_{eg,i}/e$ for all i . The condition for a nonzero inelastic current is $|eV_b| > \min [E_{eg,i}]$ which is a generalized result of the $l = 1$ model [26].

As shown in Eqs. (3) and (6), the inelastic tunneling current $I_{-,inela}$ is a convolution of the square of the molecular transition density and the wavefunctions of the electrodes. It inherits the profile of the molecular transition density in the x - y plane. Thus the molecule is more likely to get excited when the tip is above a larger transition density (absolute value). This submolecular-resolution feature has also been captured in the other two STML excitation mechanisms [21, 25, 31, 32], where only the bright-state excitation under the dipole approximation is studied. Beyond the dipole approximation, our theory predicts the dark-state excitation in the inelastic electron scattering (IES) mechanism. This discovery will provide a new platform for the study of molecular dark states.

General result of dark-state excitation – As a proof-of-principle example, we use a simplified molecule with only two levels, namely $l = 1$. The transition density is assumed to be in a Gaussian form,

$$\rho_T(\vec{r} \equiv (x, y, z)) = \frac{1}{2\pi\sigma} \left(\frac{1}{\sigma_1} e^{-\frac{x^2}{2\sigma_1^2}} - \frac{1}{\sigma_2} e^{-\frac{x^2}{2\sigma_2^2}} \right) e^{-\frac{y^2}{2\sigma^2}} \delta(z), \quad (8)$$

where $\sigma, \sigma_1, \sigma_2$ are the width of the wave packets and $\delta(z)$ is the Dirac delta function. The transition density is assumed in the x - y plane, shown in Fig. 2 (a)). The transition dipole is zero for the current dark state, i.e.,

	μ_x (a.u.)	μ_y (a.u.)	μ_z (a.u.)	$E_i - E_j$ (eV)
$S_0 - S_1(S_2)$	0.00(3.17)	3.17(0.00)	0.00	1.98
$S_0 - S_3(S_4)$	0.00	0.00	0.00	3.69
$S_0 - S_{17}$	0.00	0.00	-0.21	4.45
$S_3 - S_{17}$	0.27	0.00	0.00	0.76

Table I. The energy gap and transition dipole moments of some electronic transitions in the ZnPc molecule.

$$\int \vec{r} \rho_T(x, y, z) dx dy dz = 0.$$

In the calculation, we assume the silver tip and substrate with the Fermi energy $\mu_0 = -4.64eV$. The radius of the tip is $R = 0.5nm$, and the distance between the molecular plane and the tip is $d = 1nm$. The molecular energy gap between the ground and dark-excited state is $E_{eg} = 2eV$. Here we choose $2\sigma_1 = \sigma_2 = \sigma = 1nm$.

Fig. 2 shows the transition density (subfigure (a)) and the calculated tunneling current (subfigure (b)) from Eq. (7) with tip scanned in the x - y plane. The bias voltage is set as $V_b = -2.5V$ to allow a non-zero current. The tunneling current profile resembles that of the transition density as shown in subfigure (a) and (b). We compare the tunneling current with the transition density at the cross section along $y = 0$ and $0.4nm$ in subfigure (c). The curves show the same trend with small deviation of the positions of the minima.

The main features of the inelastic current in the IES mechanism in Ref. [26] also appears in this work that goes beyond the dipole approximation. The minimal bias for nonzero inelastic current equals the molecule energy gap divided by the electron charge. The inelastic current at negative bias is larger than that at the positive bias (see Supplementary Material). The two features are typical in the IES mechanism in the cases with or without the dipole approximation.

Excitation of dark state of ZnPc – To show its capability in practical applications, we study the excitation of a zinc-phthalocyanine (ZnPc) molecule, widely used in the STML experiments [22, 31]. Tab. (I) shows the transition dipoles and the energy gaps of the ZnPc molecule used in this paper. Due to the D_{4h} symmetry of ZnPc (see the inset in Fig. 1 (a)), its first two excited states (S_1 and S_2) whose eigenenergy is 1.98eV are doubly degenerate. Both the S_1 and S_2 states, i.e., the Q states [33, 34], are bright states, and their excitation and luminescence have already been observed in experiments. Its third and fourth eigenstates S_3 and S_4 with eigenenergy 3.69eV are degenerate dark states. The details of these eigenstates and transition dipoles are obtained with the time-dependent density functional theory (TDDFT) at

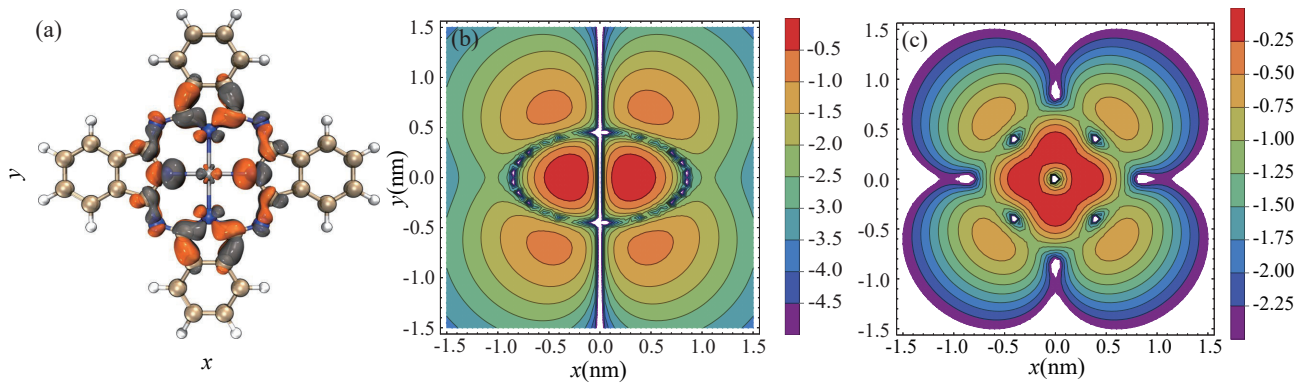


Figure 3. (a) The calculated transition density of transition between the ground state S_0 and dark state S_3 . The orange and gray parts represent the positive and negative transition density, respectively. (b) The 2D logarithmic plot of the relative inelastic current of transition between the ground state S_0 and dark state S_3 at $V_b = -4V$. (c) The 2D logarithmic plot of the sum of the relative inelastic current of transitions S_0 - S_3 and S_0 - S_4 .

ω B97X-D [35] /TZVP [36] level by Gaussian 16 program [37] and shown in Tab. (I). Fig. 3(a) shows the calculated transition density of transition between the ground state S_0 and dark state S_3 . The transition density is an even function in the y -axis and an odd function in both the x - and z -axes.

Fig. 3(b) shows the 2D logarithmic plot of the normalized inelastic current of S_0 - S_3 transition (at $V_b = -4V$). With the bias larger than the energy of the S_0 - S_3 transition, the tunneling electron in STM allows the S_0 - S_3 transition [26]. The 2D map of tunneling current are obtained by moving the tip over the molecules at the constant height $d = 1.0\text{nm}$. The plot clearly shows the two maxima and four secondary maxima in the transition density. With the same bias, the transition S_0 - S_4 is activated simultaneously. The total current as the summation of the two transitions S_0 - S_3 and S_0 - S_4 are shown in Fig. 3(c). The profile shows a four-lobe pattern which is similar to that of the bright state observed in the experiment [31].

Unlike the excitation of the molecular bright state, the molecule in its dark state can not decay to its ground state through spontaneous emission due to the optical selection rule. The lifetime of the dark state is much longer than that of the bright state. The inelastic current induced by the dark-state excitation approaches zero when the dark state is totally excited (the population of dark state is unity). The stable excitation of the dark state can be obtained with a designed cyclic scheme as follows.

Detection of dark-state excitation of ZnPc – One possible approach is to excite the dark state to a higher bright state and detect the luminescence of the bright state. To illuminate our proposal, we choose the higher bright state S_{17} with eigenenergy 4.45eV . The transition dipole of S_0 - S_{17} transition has a nonzero z -component (-0.21 a.u.), and that of S_3 - S_{17} transition has a nonzero

x -component (0.27 a.u.). Both the two transitions are optically allowed. As shown in Fig. 1 (b), the molecule in its ground state is excited to the dark state through the IES process with STM. A laser at the wavelength 1635.7nm (0.76eV) pumps the molecule resonantly from the state S_3 to state S_{17} . ZnPc in state S_{17} will emit photons at two wavelength 1635.7nm and 279.4nm (the S_0 - S_{17} transition). The luminescence photons are collected at the wavelength 279.4nm . The kinetic equations of the populations on the three states are written as

$$\begin{aligned} \dot{P}_0(t) &= -\frac{I_{ine,03}}{e}P_0(t) + \gamma_0 P_{17}(t), \\ \dot{P}_3(t) &= -\eta P_3(t) + \frac{I_{ine,03}}{e}P_0(t) + \gamma_3 P_{17}(t), \\ \dot{P}_{17}(t) &= -(\gamma_0 + \gamma_3)P_{17}(t) + \eta P_3(t), \end{aligned} \quad (9)$$

where $I_{ine,03}$ is the inelastic current of the S_0 - S_3 transition and η characterizes the transition pump rate induced by the pumping laser. And γ_0 (γ_3) is the spontaneous emission rate from the state S_{17} to the state S_0 (S_3). In the steady state, the photon emission rate from S_{17} to S_0 is

$$\Gamma = \gamma_0 P_{17,s} = \gamma_0 \frac{I_{ine,03}}{e} \left(\gamma_0 + \frac{I_{ine,03}}{e} \frac{\gamma_0 + \gamma_3 + \eta}{\eta} \right)^{-1}, \quad (10)$$

where $P_{17,s}$ is the population of state S_{17} in the steady state.

The photon emission rate in Eq. (10) approximately equals the inelastic current over an electron charge $I_{ine,03}/e$. In the STML experiment, the photon yield (luminescence probability) is as small as 10^{-5} photon/electron [38]. For the ZnPc molecule, the total excitation rate (I_{ine}/e) is estimated approximately as $1.3 \times 10^4 \text{s}^{-1}$ [26, 31]. As a result, the dark-state excitation rate $I_{ine,03}/e$ induced by the IES process should be several orders of magnitude smaller than $1.3 \times 10^4 \text{s}^{-1}$. For a moderate laser pump ($\eta \gg \gamma_0 + \gamma_3$), the second term in the

parenthesis of Eq. (10) is approximately $I_{ine,03}/e$. The emission rate of the $S_{17}-S_0$ transition reads $\gamma_0 = 4 \times 10^4 \text{s}^{-1}$ which will be much larger than the second term.

Conclusion – We propose a new perspective for STM to profile the dark-state transition density and demonstrate its capability in both the proof-of-principle example and the simulation of the practical application with the ZnPc molecule. Benefiting from the sub-nanometer resolution, STM can excite the molecular dark state beyond the dipole approximation and the inelastic current inherits the main characters of its corresponding transition density in the sub-molecular scale. The additional laser pump to the bright state allows the observation of the characteristic features in the current with photon counting. The current proposal will extend the application of STM to probe the photoprotection and energy-transfer effect on the single molecule level.

H.D. thanks the support from the NSFC (Grant No. 11875049), the NSAF (Grants No. U1730449 and No. U1930403), and the National Basic Research Program of China (Grant No. 2016YFA0301201). X.S. thanks the support from the NSFC (Grant No. 21903054).

* xiang.sun@nyu.edu

† hdong@gscaep.ac.cn

- [1] H. Haken, *Laser Theory* (Springer-Verlag, Berlin, 1984).
- [2] M. Scully and M. S. Zubairy, *Quantum optics* (Cambridge University Press, England, 1999).
- [3] E. L. Raab, M. Prentiss, A. Cable, S. Chu, and D. E. Pritchard, *Phys. Rev. Lett.* **59**, 2631 (1987).
- [4] P. D. Lett, R. N. Watts, C. I. Westbrook, W. D. Phillips, P. L. Gould, and H. J. Metcalf, *Phys. Rev. Lett.* **61**, 169 (1988).
- [5] C. N. Cohen-Tannoudji and W. D. Phillips, *Physics Today* **43**, 33 (1990).
- [6] C. E. Wieman, D. E. Pritchard, and D. J. Wineland, *Rev. Mod. Phys.* **71**, S253 (1999).
- [7] S. M. Dutra, *Cavity Quantum Electrodynamics: The Strange Theory of Light in a Box* (Wiley, New Jersey, 2005).
- [8] H. Walther, B. T. H. Varcoe, B.-G. Englert, and T. Becker, *Rep. Prog. Phys.* **69**, 1325 (2006).
- [9] G. S. Agarwal, *Quantum optics* (Cambridge University Press, New York, 2013).
- [10] B. H. Stuart, *Infrared Spectroscopy: Fundamentals and Applications* (Wiley, New Jersey, 2004).
- [11] P. Larkin, *Infrared and Raman spectroscopy* (Elsevier, Waltham, 2011).
- [12] T. Tanaka, ed., *Experimental Methods in Polymer Science* (Academic Press, San Diego, 2000).
- [13] A. Romani, C. Clementi, C. Miliani, and G. Favaro, *Acc. Chem. Res.* **43**, 837 (2010).
- [14] C. T. Middleton, K. de La Harpe, C. Su, Y. K. Law, C. E. Crespo-Hernández, and B. Kohler, *Annu. Rev. Phys. Chem.* **60**, 217 (2009).
- [15] H. Hashimoto, C. Uragami, N. Yukihiro, A. T. Gardiner, and R. J. Cogdell, *J. R. Soc. Interface* **15**, 20180026 (2018).
- [16] J. Feng, C.-W. Tseng, T. Chen, X. Leng, H. Yin, Y.-C. Cheng, M. Rohlfing, and Y. Ma, *Nat. Commun.* **8**, 71 (2017).
- [17] J. Repp, G. Meyer, S. M. Stojković, A. Gourdon, and C. Joachim, *Phys. Rev. Lett.* **94**, 026803 (2005).
- [18] C. Chen, P. Chu, C. A. Bobisch, D. L. Mills, and W. Ho, *Phys. Rev. Lett.* **105**, 217402 (2010).
- [19] A. Rosławska, P. Merino, C. Große, C. C. Leon, O. Gunnarsson, M. Etzkorn, K. Kuhnke, and K. Kern, *Nano Lett.* **18**, 4001 (2018).
- [20] L. L. Nian, Y. Wang, and J. T. Lü, *Nano Lett.* **18**, 6826 (2018).
- [21] H. Imada, K. Miwa, M. Imai-Imada, S. Kawahara, K. Kimura, and Y. Kim, *Phys. Rev. Lett.* **119**, 013901 (2017).
- [22] B. Doppagne, M. C. Chong, H. Bulou, A. Boeglin, F. Scheurer, and G. Schull, *Science* **361**, 251 (2018).
- [23] G. Chen, Y. Luo, H. Y. Gao, J. Jiang, Y. J. Yu, L. Zhang, Y. Zhang, X. G. Li, Z. Y. Zhang, and Z. C. Dong, *Phys. Rev. Lett.* **122**, 177401 (2019).
- [24] J. Kröger, B. Doppagne, F. Scheurer, and G. Schull, *Nano Lett.* **18**, 3407 (2018).
- [25] X. Y. Wu, R. L. Wang, Y. Zhang, B. W. Song, and C. Y. Yam, *J. Phys. Chem. C* **123**, 15761 (2019).
- [26] G. Dong, Y. You, and H. Dong, *New J. Phys.* **22**, 113010 (2020).
- [27] J. Bardeen, *Phys. Rev. Lett.* **6**, 57 (1961).
- [28] A. D. Gottlieb and L. Wesolowski, *Nanotechnology* **17**, R57 (2006).
- [29] J. Tersoff and D. R. Hamann, *Phys. Rev. Lett.* **50**, 1998 (1983).
- [30] J. Tersoff and D. R. Hamann, *Phys. Rev. B* **31**, 805 (1985).
- [31] Y. Zhang, Y. Luo, Y. Zhang, Y. J. Yu, Y. M. Kuang, L. Zhang, Q. S. Meng, Y. Luo, J. L. Yang, Z. C. Dong, and J. G. Hou, *Nature (London)* **531**, 623 (2016).
- [32] F.-F. Kong, X.-J. Tian, Y. Zhang, Y.-J. Yu, S.-H. Jing, Y. Zhang, G.-J. Tian, Y. Luo, J.-L. Yang, Z.-C. Dong, and J. G. Hou, *Nat. Commun.* **12**, 1280 (2021).
- [33] L. Edwards and M. Gouterman, *J. Mol. Spectrosc.* **33**, 292 (1970).
- [34] G. Ricciardi, A. Rosa, and E. J. Baerends, *J. Phys. Chem. A* **105**, 5242 (2001).
- [35] J.-D. Chai and M. Head-Gordon, *Phys. Chem. Chem. Phys.* **10**, 6615 (2008).
- [36] A. Schäfer, C. Huber, and R. Ahlrichs, *J. Chem. Phys.* **100**, 5829 (1994).
- [37] M. J. Frisch *et al.*, *Gaussian 16 Rev. B.01* (Gaussian, Inc., Wallingford, CT, 2016).
- [38] M. C. Chong, *Electrically driven fluorescence of single molecule junctions*, *Ph.D. thesis*, Université de Strasbourg, France (2016).

where \hat{P}_k is the k -th permutation operators, $(-1)^P$ is $+1$ for an even permutation and -1 for an odd permutation, the summation contains all the permutations, and $\Pi = 1/\sqrt{(2N)!}$ is the normalization factor.

In the sub-space of the ground state Ψ_G and excited state $|\Psi_{E,i}\rangle$ ($i = 1, \dots, l$), we find the coupling term as

$$\begin{aligned}
\hat{H}_{\text{el-m}} &= \left(|\Psi_G\rangle \langle \Psi_G| + \sum_{i=1}^l |\Psi_{E,i}\rangle \langle \Psi_{E,i}| \right) \left(\sum_{p=1}^n \frac{Z_n e^2}{|\hat{r}_0 - \hat{R}_p|} - \sum_{q=1}^{2N} \frac{e^2}{|\hat{r}_0 - \hat{r}_q|} \right) \left(|\Psi_G\rangle \langle \Psi_G| + \sum_{j=1}^l |\Psi_{E,j}\rangle \langle \Psi_{E,j}| \right) \\
&= \sum_{p=1}^n \frac{Z_n e^2}{|\hat{r}_0 - \hat{R}_p|} - \sum_{q=1}^{2N} \left(\sum_{i,j=1}^l \langle \Psi_{E,i}| \frac{e^2}{|\hat{r}_0 - \hat{r}_q|} |\Psi_{E,j}\rangle |\Psi_{E,i}\rangle \langle \Psi_{E,j}| + \langle \Psi_G| \frac{e^2}{|\hat{r}_0 - \hat{r}_q|} |\Psi_G\rangle |\Psi_G\rangle \langle \Psi_G| \right) \\
&\quad - \frac{2N}{(2N)!} \sum_{i=1}^l \left(\langle \Psi_{E,i}| \frac{e^2}{|\hat{r}_0 - \hat{r}_1|} |\Psi_G\rangle |\Psi_{E,i}\rangle \langle \Psi_G| + \langle \Psi_G| \frac{e^2}{|\hat{r}_0 - \hat{r}_1|} |\Psi_{E,i}\rangle |\Psi_G\rangle \langle \Psi_{E,i}| \right) \\
&= \sum_{p=1}^n \frac{Z_n e^2}{|\hat{r}_0 - \hat{R}_p|} - \sum_{q=1}^{2N} \left(\sum_{i,j=1}^l \langle \Psi_{E,i}| \frac{e^2}{|\hat{r}_0 - \hat{r}_q|} |\Psi_{E,j}\rangle |\Psi_{E,i}\rangle \langle \Psi_{E,j}| + \langle \Psi_G| \frac{e^2}{|\hat{r}_0 - \hat{r}_q|} |\Psi_G\rangle |\Psi_G\rangle \langle \Psi_G| \right) \\
&\quad - \frac{2N}{(2N)!} \sum_{i=1}^l \left((2N-1)! \langle \chi_{e,i}| \frac{e^2}{|\hat{r}_0 - \hat{r}_1|} |\chi_g\rangle |\Psi_{E,i}\rangle \langle \Psi_G| + (2N-1)! \langle \chi_g| \frac{e^2}{|\hat{r}_0 - \hat{r}_1|} |\chi_{e,i}\rangle |\Psi_G\rangle \langle \Psi_{E,i}| \right) \\
&= \sum_{p=1}^n \frac{Z_n e^2}{|\hat{r}_0 - \hat{R}_p|} - \sum_{q=1}^{2N} \left(\sum_{i,j=1}^l \langle \Psi_{E,i}| \frac{e^2}{|\hat{r}_0 - \hat{r}_q|} |\Psi_{E,j}\rangle |\Psi_{E,i}\rangle \langle \Psi_{E,j}| + \langle \Psi_G| \frac{e^2}{|\hat{r}_0 - \hat{r}_q|} |\Psi_G\rangle |\Psi_G\rangle \langle \Psi_G| \right) \\
&\quad - \sum_{i=1}^l \int d^3 \vec{r} \frac{e^2 \rho_{T,i}(\vec{r})}{|\hat{r}_0 - \vec{r}|} (|\Psi_{E,i}\rangle \langle \Psi_G| + |\Psi_G\rangle \langle \Psi_{E,i}|), \tag{2}
\end{aligned}$$

where we have defined transition density $\rho_{T,i}(\vec{r}) = \chi_{e,i}^*(\vec{r}) \chi_g(\vec{r}) = \chi_g^*(\vec{r}) \chi_{e,i}(\vec{r})$ [1].

The last term in Eq. (2) represents the molecular transition between its ground and excited states. In the single-electron Hilbert space, we rewrite the last term of the interaction Hamiltonian as

$$\hat{H}_{\text{el-m}} \simeq - \sum_{i=1}^l \int d^3 \vec{r} \frac{e^2 \rho_{T,i}(\vec{r})}{|\hat{r}_0 - \vec{r}|} (|\chi_{e,i}\rangle \langle \chi_g| + |\chi_g\rangle \langle \chi_{e,i}|)$$

Thus, in the main text we focus on the calculation of this term. The transition matrix element of transition $|\chi_{e,i}\rangle |\varphi_n\rangle \rightarrow |\chi_g\rangle |\phi_{k_0}\rangle$ (negative bias) is

$$\begin{aligned}
\mathcal{N}_{s,t;i|-V_b, E_n \rightarrow \xi_{k_0}} &= \int d^3 \vec{r}_0 \int d^3 \vec{r} \frac{\rho_{T,i}(\vec{r}) e^2}{|\vec{r}_0 - \vec{r}|} \varphi_n(\vec{r}_0) \phi_{k_0}(\vec{r}_0) \\
&= \int d^3 \vec{r}_0 \int d^3 \vec{r} \frac{\rho_{T,i}(\vec{r}) e^2}{|\vec{r}_0 - \vec{r}|} \rho_{n,k_0}(\vec{r}_0) \\
&= \frac{1}{(2\pi)^3} \int d^3 \vec{r}_0 \int d^3 \vec{r} \int \int d^3 \vec{p} d^3 \vec{q} \frac{\rho_{T,i}(\vec{q}) e^2}{|\vec{r}_0 - \vec{r}|} \rho_{n,k_0}(\vec{p}) e^{-i\vec{p} \cdot (\vec{r}_0 - \vec{r})} e^{-i(\vec{p} + \vec{q}) \cdot \vec{r}} \\
&= \frac{1}{(2\pi)^3} \int d^3 \vec{r}_0 \int d^3 \vec{r} \int \int d^3 \vec{p} d^3 \vec{q} \frac{\rho_{T,i}(\vec{q}) e^2}{|\vec{r}_0|} \rho_{n,k_0}(\vec{p}) e^{-i\vec{p} \cdot \vec{r}_0} e^{-i(\vec{p} + \vec{q}) \cdot \vec{r}} \\
&= \int d^3 \vec{r}_0 \int \int d^3 \vec{p} d^3 \vec{q} \frac{\rho_{T,i}(\vec{q}) e^2}{|\vec{r}_0|} \rho_{n,k_0}(\vec{p}) e^{-i\vec{p} \cdot \vec{r}_0} \delta(\vec{p} + \vec{q}) \\
&= \int d^3 \vec{q} \rho_{T,i}(\vec{q}) \rho_{n,k_0}(-\vec{q}) \left[\int d^3 \vec{r} \frac{e^2}{|\vec{r}|} e^{i\vec{q} \cdot \vec{r}} \right] \\
&= e^2 \int d^3 \vec{q} \rho_{T,i}(\vec{q}) \rho_{n,k_0}(-\vec{q}) \frac{4\pi}{q^2}, \tag{3}
\end{aligned}$$

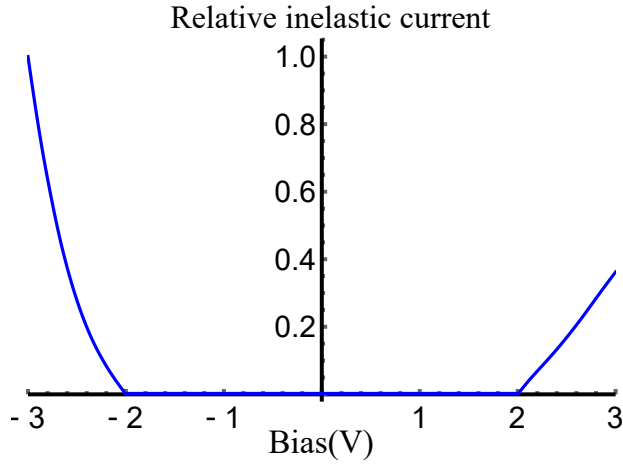


Figure 2. (Color online) The relative inelastic current when the tip is placed right above point $(0,0)$. Here we choose $2\sigma_1 = \sigma_2 = \sigma = 1\text{nm}$, $R = 0.5\text{nm}$, $d = 1\text{nm}$, and $E_{eg} = 2\text{eV}$.

where we have used the notation $\rho_{n,k_0}(\vec{r}) = \varphi_n(\vec{r})\phi_{k_0}(\vec{r})$, and $\rho_{T,i}(\vec{k}), \rho_{n,k_0}(\vec{k})$ are the Fourier transformations of $\rho_{T,i}(\vec{r}), \rho_{n,k_0}(\vec{r})$

$$\rho_{T,i}(\vec{k}) = \frac{1}{\sqrt{2\pi}^3} \int d^3\vec{r} \rho_{T,i}(\vec{r}) e^{i\vec{k}\cdot\vec{r}}, \quad (4)$$

$$\rho_{n,k_0}(\vec{k}) = \frac{1}{\sqrt{2\pi}^3} \int d^3\vec{r} \varphi_n(\vec{r}) \phi_{k_0}(\vec{r}) e^{i\vec{k}\cdot\vec{r}}. \quad (5)$$

II. CURRENT AT POSITIVE BIAS

For the positive bias, the inelastic current has a similar form which is

$$I_{+,inela} \simeq \sum_{i=1}^l I_{+,inela,i}, \quad (6)$$

where

$$I_{+,inela,i} = 2\pi e \int_{\mu_0}^{\mu_0 + eV_b - E_{eg,i}} dE_n \rho_s(E_n) \rho_t(\xi_k) \times |\mathcal{N}_{t,s;i}|_{V_b, \xi_k \rightarrow E_n}|_{\xi_k = E_n - eV_b + E_{eg,i}}|^2. \quad (7)$$

III. ASYMMETRY OF CURRENT

We study the inelastic current of the Gaussian transition density for different bias voltage. Fig. 2 depicts the variation of the inelastic current as a function of bias voltage. Here we choose that both the tip and substrate are made of silver, and the Fermi energy is $\mu_0 = -4.64\text{eV}$. The radius of the tip is $R = 0.5\text{nm}$, and the distance between the molecular plane and tip is $d = 1\text{nm}$. The energy gap between the molecular ground state and dark excited state is $E_{eg} = 2\text{eV}$. Without the loss of generality, we choose the tip to be right above the center of the molecular transition density, namely $A = (0,0)$. Fig. 2 shows that when the bias voltage is larger than the molecular energy gap ($|eV_b| > E_{eg}$), the inelastic current becomes nonzero. Moreover, the inelastic current at negative bias is larger than that at positive bias. Actually, these two features are also found in the study of inelastic electron scattering mechanism under the dipole approximation [2]. These two features are typical in the IES mechanism in the cases with or without the dipole approximation.

IV. EXCITATION OF ZNPC BRIGHT STATE

As shown in the main text, the total inelastic current of the system consists of the contribution of all the transitions whose transition energy is lower than eV_b . Without loss of generality, here we choose a negative bias $V_b = -2.5V$. At $V_b = -2.5V$, the total inelastic current is the sum of the current induced by transitions S_0 - S_1 and S_0 - S_2 .

Fig. 3(a) depicts the transition density of transition between the ground state S_0 and bright state S_1 . The transition density is an odd function in the y -axis and an even function in both the x - and z -axes, which gives a nonzero transition dipole moment in the y -axis. Fig. 3(b) plots the 2D logarithmic plot of the normalized inelastic current (luminescence strength) of S_0 - S_1 transition. As the transition dipole lies along the y -axis, the inelastic current gives a two-spot pattern along the y -axis. The inelastic current (luminescence strength) around the x -axis is smaller than that along the y -axis by several orders of magnitude and thus is undetectable. Due to the symmetry of the ZnPc molecule, the transition density of S_0 - S_2 transition can be obtained by rotating the Fig. 3(a) 90° along the z -axis. The total inelastic current (luminescence strength) contributed by S_0 - S_1 and S_0 - S_2 transition is shown in Fig. 3(c). We can see that the total current inherits the four-lobe pattern from the geometric symmetry of the ZnPc, which has been observed in experiments [3, 4].

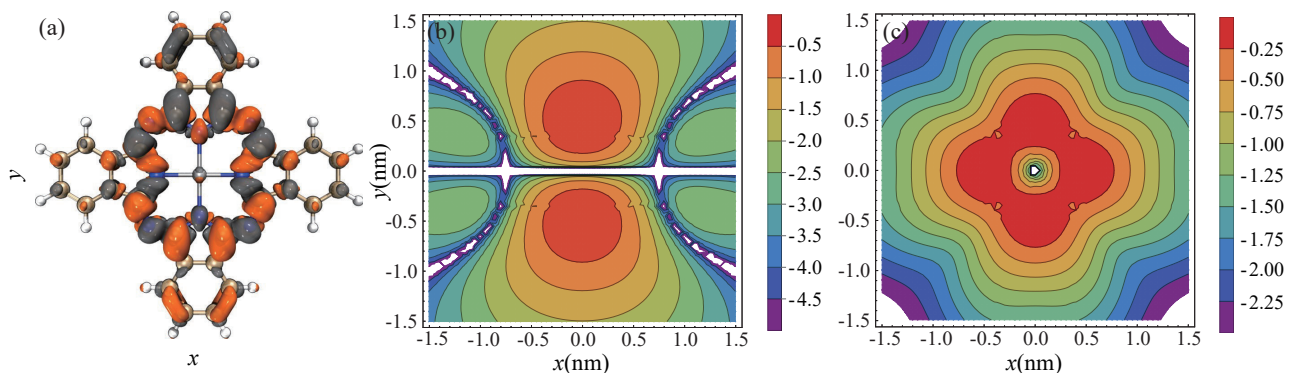


Figure 3. (a) The transition density of transition between the ground state S_0 and bright state S_1 . (b) The 2D logarithmic plot of the relative inelastic current of transition between the S_0 and S_1 at $V_b = -2.5V$. (c) The 2D logarithmic plot of the sum of the relative inelastic current of transitions S_0 - S_1 and S_0 - S_2 .

* xiang.sun@nyu.edu

† hdong@gscaep.ac.cn

- [1] M. Sun, J. Chen, and H. Xu, *J. Chem. Phys.* **128**, 064106 (2008).
- [2] G. Dong, Y. You, and H. Dong, *New J. Phys.* **22**, 113010 (2020).
- [3] Y. Zhang, Y. Luo, Y. Zhang, Y. J. Yu, Y. M. Kuang, L. Zhang, Q. S. Meng, Y. Luo, J. L. Yang, Z. C. Dong, and J. G. Hou, *Nature (London)* **531**, 623 (2016).
- [4] Y. Luo, G. Chen, Y. Zhang, L. Zhang, Y. J. Yu, F. F. Kong, X. J. Tian, Y. Zhang, C. X. Shan, Y. Luo, J. L. Yang, V. Sandoghdar, Z. C. Dong, and J. G. Hou, *Phys. Rev. Lett.* **122**, 233901 (2019).